Improving Tumoral Acidic pH-Responsive Drug Efficiency Based on GO@Au Nanocomposite

Mingqing Tang (TMQ@hqu.edu.cn)
School of Medicine, Huaqiao University
Pengliang Xin
Quanzhou First Hospital Affiliated to Fujian Medical University
Hongjun Lin
School of Medicine, Huaqiao University
Huangen Li
Quanzhou First Hospital Affiliated to Fujian Medical University

Research

Keywords: Tumor, Photothermal, Chemotherapy, Drug delivery

Posted Date: August 18th, 2020

DOI: https://doi.org/10.21203/rs.3.rs-57457/v1

Abstract

Background: to accurately deliver drugs to the lesion site and realize its timed and quantitative release is the focus of tumor therapy. In this paper, a tumor targeted near-infrared light controlled release drug delivery system integrating hyperthermia and chemotherapy was successfully constructed by combining tumor hyperthermia and chemotherapy.

Results: by hydrothermal method, Au nanoparticles were firstly loaded onto the GO surface to obtain GO@Au nanocomposites, then PEG was loaded onto the GO@Au by pH sensitive hydrazone bond to obtain GO@Au-PEG, and DOX is finally loaded onto the GO surface via π-π stacking. The target controlled release drug delivery system showed good tumor targeting property, can be the efficient transfer of drug to the tumor cells, and the tumor cells in near-infrared light control of DOX release. In vivo tumor inhibition experiments in mice, the targeted drug delivery system showed obvious tumor inhibition characteristics and had good effects of hyperthermia and chemotherapy.

Conclusions: therefore, this tumor targeted near-infrared controlled release drug delivery system has great potential in tumor therapy.

1 Background

Cancer has become one of the major diseases threatening human life[1-4]. At present, chemotherapy is still an indispensable and important means in the treatment of cancer. However, due to the poor specificity of chemotherapy drugs to tumor tissues, it has great toxic and side effects, so its therapeutic effect is not ideal[5]. Using nanomaterials as drug carriers to construct a chemotherapeutic drug controlled release system can reduce the toxic and side effects of chemotherapeutic drugs and improve their efficacy[6-9] .

The appearance of controlled release drug delivery system is expected to solve the shortcomings of poor specificity of chemotherapy and high toxic and side effects[10-12] . It enables drugs to be released as much as possible at the site of disease, and can maintain the effective therapeutic concentration of drugs at the site of disease, while remaining within the safe concentration range in other tissues[13]. Therefore, the toxic and side effects of chemotherapy drugs can be reduced and the curative effect can be improved.

Stimuli-responsive controlled release drug delivery system is an intelligent drug delivery system, which refers to the drug delivery system in the external environment or the human body's own environmental factors (pH, temperature, light, enzyme and ion intensity, etc.) under the stimulation of some physical or chemical changes, so as to achieve the controlled release of drug delivery system[14-17]. A wide range of stimuli-responsive controlled release drug delivery systems have been studied, including pH responsive controlled release drug delivery system, temperature responsive controlled release drug delivery system and photothermal response controlled release drug delivery system[18-20] .

The use of thermotherapy to treat cancer has also attracted a lot of attention. High temperatures can cause cancer cells to die, and when the temperature rises above 42℃, overheating can cause damage to the cells. Photothermal therapy has attracted wide attention in recent years and is regarded as one of the most promising tumor treatment technologies, because of its controllable, minimally invasive and efficient tumor treatment advantages[21-23]. But a big disadvantage of this approach is the lack of specificity. As the temperature of the tumor area rises, other surrounding tissues may also be damaged by the high temperature[24].

Combining nanomaterials with chemotherapeutic drugs to construct a tumor targeting drug delivery system can realize the synergistic effect of chemotherapy and hyperthermia on tumors. In order to integrate various functions into a single structure to match the treatment process, many people have been working to develop hybrid nanosystems[25-28]. Despite the exciting recent progresses in the development of multi-functional drug delivery system. However, more effective tumor targeting drug delivery systems need to be developed to enable the coordinated treatment of cancer with chemotherapy and hyperthermia.

In the current study, a new doxorubicin (DOX) , one of the most effective drugs against a wide range of cancers, delivery system with pH sensitivity and photodynamic therapy was designed, synthesized, characterized and explored for its potential applications both in drug delivery and in photodynamic therapy. Firstly, graphene oxide (GO) and gold (Au) bybrid nanocomposite is synthesized. The composite is functionalized by polyethylene glycol (PEG2000). Then DOX was employed as the model drug and loaded onto GO@Au-PEG with high efficacy. The new drug delivery system is characterized by transmission electron microscopy (TEM), dynamic laser scattering (DLS), Fourier transmission infrared spectroscopy (FTIR) and UV spectrums. The tumor diagnostic and positioning ability, tumor-targeting property, photothermal therapy (PTT) and combination therapeutic efficacy of GO@Au-PEG/DOX was evaluated.

2 Materials

2.1 Materials

Table 1 shows the main materials used in this paper. Sodium citrate, Anhydrous ethanol, Dimethylformamide (DMF), Pyridine, 4-dimethylaminopyridine (DMAP), P-nitrophenyl chloroformate, Hexamethylene diamine, Carbodiimide hydrochloride (EDC·HCl), P-hydroxybenzoic acid (HBA), Potassium bromide (KBr), Sodium chloride (NaCl), Sodium dihydrogen alkenate, Disodium hydrogen phosphate, phosphate buffered asline (PBS) etc are also used in this study.

Table 1 The main materials used in this paper.

Materials	GO	DOX 20180503	$HAuCl_4$	CHO-PEG2000
Purity	>95%	>98%	>99%	>98%
From	Shanghai Alighting Biochemical Technology Co. Ltd.	Beijing Yi-He Biotech Co. Ltd.	Shanghai Alighting Biochemical Technology Co. Ltd.	Xi 'an Ruixi Biological Technology Co. Ltd.

2.2 Synthesis of GO@Au

Weigh 50 mg GO, place it in a small beaker, add 150 ml ultra-pure water, and ultrasound makes it completely dispersed. In the dark condition, 10 ml $HAuCl_4$ (0.025 M) solution was added while shaking, and then 10 ml sodium citrate solution (0.1 M) was added to the mixed solution. After ultrasonic mixing for 10 min, the solution was transferred to the reactor and reacted at 120 ℃ for 10 h. At the end of the reaction, the reaction products were naturally cooled to room temperature, centrifuged at 12000 rpm for 10 min, then the precipitation was washed for 3 times with ultrapure water and anhydrous ethanol, and dried in a vacuum at 60 ℃ for 12 h to obtain GO@Au nanocomposites.

2.3 Synthesis of GO@Au-PEG/DOX

Put 50 mg GO@Au powder in a three-mouth flask, and an appropriate amount of DMF was added, followed by ultrasonic cleaning until the powder was completely dispersed, and then 2 ml pyridine, 20 mg DMAP and 400 mg P-nitrophenyl chloroformate were added. The powder was then reacted in a water bath at 0℃ under the protection of nitrogen, and stirred for 48h (ultrasonic treatment1 h per 8 h). At the end of the reaction, diethyl ether was added to the reaction system to precipitate the black substance. The reaction product was repeatedly washed step by step with diethyl ether, dichloromethane and isopropanol. Put the product into vacuum drying at 60 ℃ for 12h to obtain activated GO@Au. 50 mg activated GO@Au were dispersed in DMF and treated with ultrasonic under nitrogen protection for 30 min to disperse them. Then 10 ml ethylenediamine and 2 ml diisopropyl ethylamine were added and stirred at room temperature for 24h. Then it was cleaned with methanol and pure water and dried at 60℃ for 12h to obtain GO@Au-NH_2.

50 mg GO@Au-NH_2 and 50 mg HBA were dissolved in PBS (pH 7.4), then EDC·HCL 80 mg and NHS 35 mg were added and stirred at room temperature for 48 h. At the end of the reaction, 200 ml ethanol was added, then the precipitate was washed with ethanol. Finally GO@Au-HBA was obtained by vacuum drying at 60℃ for 12h. 50 mg GO@Au-HBA and 200 mg CHO-PEG200 were mixed in 50 ml DMSO at room temperature and in darkness for 24 h, and then dialyzed (MWCO=10000) in deionized water with dialysis membrane for 3 days. Finally, the solution was freeze-dried to obtain GO@Au-PEG. At the same time, synthesis of GO@Au-PEG* without pH sensitive hydrazone bond for comparison experiment.

GO@Au-PEG (50 mg) and DOX (100 ml) were added to DMSO (50 ml) stirred at room temperature in the dark for 24 h. Then the nanosuspension was centrifuged to remove free DOX. After freeze-drying, the solid products GO@Au-PEG/DOX were dried in vacuum at 30 ℃ for 24 h and stored at 4℃ until use. **Figure 1** shows the schematic of the synthetic steps from GO to GO@Au-PEG/DOX.

3 Results And Discussion

3.1 Synthesis of GO@Au-PEG/DOX

Figure 1 shows the synthesis scheme of GO@Au-PEG/DOX. During the synthesis of GO@Au, mild sodium citrate was selected as the reducing agent in the experiment, and gold nanoparticles were loaded on the surface of GO by hydrothermal method to form GO@Au nanocomposite. In GO@Au-PEG synthesis process, chloroformic acid p-nitrophenyl ester was used to activate the hydroxyl group on the GO surface, to get GO@Au of nitro phenyl acetic derivatives, then connect ethylenediamine chemical by ester bond on the GO@Au nanocomposites, to form the GO@Au-NH_2, then introduced with hydrazine base HBA, add CHO-PEG2000, modified PEG by pH sensitive hydrazone bond on GO@Au nanocomposites. DOX is efficiently loaded onto the GO@Au-PEG surface through a strong π-π stacking.

3.2 Characterization of GO@Au-PEG

Figure 2a and **b** shows the TEM image of GO and GO@Au. It can be seen that GO is a typical stratified structure and Au is a sphere with a diameter of 10~20 nm. Au nanoparticles were uniformly distributed on the GO sheets, indicating that Au was successfully loaded on the GO@Au nanocomposite. **Figure 2c** shwos the UV spectrum of the GO and GO@Au. The the UV spectrum of GO@Au showed a strong absorption at 527 nm, showing that the gold nanoparticles are indeed loaded on the GO surface.

The FT-IR spectrum of GO, GO@Au, activated GO@Au, GO@Au-NH_2, GO@Au-HBA and GO@Au-PEG are show in **Figure 2d**. GO shows an obvious absorption peak at 1710 cm^{-1}, which is the absorption peak of -COOH carbonyl, and a strong absorption peak at 3400 cm^{-1}, which is the characteristic peak of -OH. GO@Au shows an obvious absorption peak at 3400 cm^{-1}, which means there remains a lot of -OH that can react with -OH on GO. When nitrophenyl was introduced and activated GO-Au was obtained, the -OH absorption peak was significantly weakened and N-O absorption peak appeared (1382 cm^{-1}), indicating that nitrophenyl was successfully attached to GO@Au. Then, after ethylenediamine is conjugated on the activated GO@Au by an ester bond, the characteristic absorption peak of C-N appears at 1140 cm^{-1}, the absorption peak of N-H bond appears at 1624 cm^{-1} and 3400 cm^{-1}, and the absorption peak of N-O bond at 1382 cm^{-1} weakens, indicating the successful synthesis of GO@AU-NH_2. When -NH_2 is introduced into GO@Au, the HBA links to GO@Au through the reaction between -COOH and -NH_2 to form amide bonds. Compared with GO@Au-NH_2, GO@Au-HBA has absorption peaks at 1661 cm^{-1} and 1388 cm^{-1}. Meanwhile, the absorption peaks of -NH_2 at 1600 cm^{-1} and 992 cm^{-1} prove the existence of N-N bonds, indicating the successful synthesis of GO@Au-HBA. Finally, CHO-PEG2000 generates pH-sensitive hydrazone by

reaction of aldehyde group with hydrazine group on HBA, and absorption peaks appear at 1716 cm^{-1} ,1241 cm^{-1} and 1600 cm^{-1}, indicating successful preparation of GO@Au-PEG.

3.3 Characterization of GO@Au-PEG/DOX

As shown in **Figure 3a**, DOX has strong absorption peaks at 252 nm and 480 nm, GO@Au-PEG has a strong absorption peak at 527 nm, GO@Au-PEG/DOX has strong absorption peaks at 252, 480 and 527 nm. The mean Zeta potential of GO@Au-PEG/DOX was 35.5±2.6 mV, indicating that the Zeta potential of GO@Au-PEG/DOX was stable.

GO@Au, GO@Au-PEG and GO@Au-PEG/DOX are all well dispersed in water. After one week of placement, the GO@Au sample had partial precipitation, while the Go@Au-PEG sample had no aggregation precipitation. This indicates that PEG improves the water solubility of GO@Au. In addition, GO@Au-PEG and GO@Au-PEG/DOX was stable in normal saline, medium, fetal bovine serum and PBS solution, and will not accumulate for several weeks.

3.4 Photothermal effect and pH sensitivity

The heating condition of GO@Au under 808 nm laser is shown in **Figure 4a**. When the water is irradiated by 808 nm laser, the temperature is almost unchanged and there is no obvious thermal effect. The solution temperature of GO and GO@Au increased significantly under the irradiation of 808 nm laser, and the heating efficiency of GO@Au solution was much higher than that of GO solution. This indicates that Au nanoparticles loaded on the GO surface significantly improve the heating efficiency.

The pH sensitivity of PEG in GO@Au-PEG is caused by the break of hydrazone bond in acidic environment, and its pH sensitivity in vitro is shown in **Figure 4b**. According to the TGA results, the PEG content in GO@Au-PEG nanocomposite was 18.0%. After incubating it in pH 7.4 phosphate buffer solution for 4 h, there was no significant change in PEG content, while after incubating it in pH 5.5 phosphate buffer solution for 4 h, the PEG remaining on GO@Au was only 2.2%. The PEG content of GO@Au-PEG* (without pH sensitivity hydrazone bond) in the control group was 23.8% and 19.6%, respectively, after incubation for 4 h in phosphoric acid buffer solution pH 7.4 and pH 5.5, with no significant change. It is safely to draw the conclusion that PEG in GO@Au-PEG has obvious pH sensitivity.

3.5 GO@Au-PEG/DOX near infrared controlled release

The absorbance of free DOX can be measured by ultraviolet spectrophotometry, and then the content of free DOX can be obtained according to the standard curve. Then the DOX in GO@Au-PEG/DOX can be obtained by difference method, thus the drug loading rate of GO@Au-PEG/DOX can be measured as about 83%.

Photostimulation is an effective stimulus to achieve controlled drug release. In this study, 808 nm laser irradiation of GO@Au was used to generate near-infrared light and release DOX from go@Au-PEG /DO drug delivery system. As shown in **Figure 5**, under laser irradiation, the DOX release rate from GO@Au-

PEG/DOX is very fast. When there is no laser irradiation, the release rate of DOX slows down significantly. At the same time, in the presence of laser irradiation, the DOX release rate of pH 5.5 group was significantly faster than that of pH 7.4 group. This indicates that laser irradiation under acidic conditions is conducive to the rapid release of DOX, which can release 80.1%.

3.6 Cellure uptake

The uptake of MCF-7 cells into the GO@Au-PEG/DOX controlled release system and the near-infrared controlled release of DOX by the system were studied using the red fluorescence DOX as the marker. As shown in **Figure 6**, GO@Au-PEG/DOX group and GO@Au-PEG*/DOX group after 4 h incubation in the complete medium pH7.4, only very weak burning red light signals, shows that only a tiny amount of DOX into MCF-7 cell. The GO@Au after PEG modification, big space steric of PEG seriously hindered the MCF-7 cell uptake of drug delivery system. Compared with the GO@Au-PEG/DOX (pH7.4) group, the uptake of MCF-7 cells was much faster in the GO@Au-PEG/DOX (pH5.5) group, because PEG was removed due to the pH5.5 rupture of pH-sensitive hydrazone bonds in the weakly acidic environment (pH5.5), and the uptake of GO@Au-PEG/DOX by McF-7 cells was accelerated. GO@Au-PEG*/DOX (without pH-sensitive hydrazone bonds) did not have this sensitivity, and uptake by MCF-7 cells did not differ significantly between pH 7.4 and pH 5.5. Once inside the cell, DOX is quickly transferred to the nucleus, where it inserts into the DNA and interferes with its synthesis, killing tumor cells. According to **Figure 6**, the red and yellow light in the GO@Au-PEG/DOX (pH 5.5) group after incubation for 4 h was mainly concentrated in the cytoplasm, indicating that a large amount of DOX was not released from the GO@Au-PEG/DOX drug delivery system. However, when the GO@Au-PEG/DOX (pH 5.5) group entered the cells at 4 h and was irradiated with 808 nm laser for 10 min, strong red light appeared in the nucleus, because the 808 nm laser radiation accelerated the release of a large amount of DOX from the GO@Au-PEG/DOX and the released DOX was transferred to the nucleus quickly. The above results indicated that the weakly acidic environment was conducive to the uptake of GO@Au-PEG/DOX by MCF-7 cells, and the controlled release of DOX by GO@Au-PEG/DOX drug delivery system could be realized by 808 nm laser irradiation group after incubation for 4 h was mainly concentrated in the cytoplasm, indicating that a large amount of DOX was not released from the GO@Au-PEG/DOX drug delivery system. However, when the GO@Au-PEG/DOX (pH5.5) group entered the cells at 4 h and was irradiated with 808 nm laser for 10 min, strong red light appeared in the nucleus, because the 808 nm laser radiation released a large amount of DOX from the Go@Au-PEG/DOX controlled release drug delivery system and was transferred to the nucleus quickly. The above results indicated that the weakly acidic environment was conducive to the uptake of GO@Au-PEG/DOX by MCF-7 cells, and the controlled release of DOX by GO@Au-PEG/DOX drug delivery system could be realized by 808 nm laser irradiation.

3.7 Cytotoxicity of GO@Au-PEG

The effects of GO, GO@Au and Go@Au-PEG at different concentrations on McF-7 cells after 24 h were shown in **Figure 7a**. As can be seen from the figure, with the increase of GO, go@Au and Go@Au-PEG concentration, the inhibition effect on MCF-7 cells was gradually presented to a certain extent. However,

when the concentration of GO, GO@Au and GO@Au-PEG was 100 μg/ml, the inhibition rate of the cells was still less than 15%, indicating that GO, GO@Au and GO@Au-PEG had no obvious toxicity on MCF-7 cells.

Figure 7b shows the effects of GO and G0@AU-PEG at different concentrations on MCF-7 cell growth without and with laser irradiation. In the absence of laser irradiation, the two drugs had little inhibitory effect on cell growth. Under laser irradiation, the growth inhibition of MCF-7 cells in GO group and GO@Au-PEG group increased with the increase of concentration. In addition, at the same concentration, the GO@Au-PEG group had more significant inhibition on cell growth than the GO group, indicating that GO@Au-PEG had stronger photohyperthermia effect under laser irradiation and had a good hyperthermia killing effect.

3.8 Inhibitory effect of GO@Au-PEG/DOX on MCF cell growth

Figure 8 shows the inhibitory effect of DOX and GO@Au-PEG/DOX at different concentrations on the growth of MCF-7 cells under laser and laser-free conditions.As shown in the figure, the growth inhibition of both DOX and GO@Au-PEG/DOX on MCF-7 cells increased with the increase of its concentration. Meanwhile, in the absence of laser irradiation, the growth inhibition effect of DOX at all concentrations on MCF-7 was higher than that of GO@Au-PEG/DOX, which was caused by the slow release of DOX from GO@Au-PEG/DOX. However, under laser irradiation, the growth inhibition of MCF-7 cells by high concentration of GO@Au-PEG/DOX was significantly enhanced, but the effect was not obvious at low concentration, because the heat generated by GO@Au at low concentration was less and could not kill the tumor cells. When DOX concentration was 10 μg/ml, the survival rate of MCF-7 cells in the GO@Au-PEG/DOX group under laser irradiation was only about 10%. This is because both hyperthermia and chemotherapy enhance the therapeutic effect at the same time, the laser promotes the release of DOX, again enhancing the therapeutic effect.

3.9 Tumor growth inhibition in vivo.

In order to investigate the anti-tumor activity of GO@Au-PEG/DOX in vivo, S180 tumor-bearing mice were used as the animal model in this chapter to investigate the tissue distribution characteristics and pharmacodynamic characteristics of the mice.

Several successful tumor-bearing mice were given free water and fasted for 12 hours. Their main organs (heart, liver, spleen, lung, kidney and tumor) and blood were collected separately and weighed, then saline was added to each sample (saline weight: organ weight = 1:1) and homogenized. CO@Au-PEG/DOX (5 mg) was dispersed in 1 ml of water and placed in a dialysis bag. The dialysis bag was then immersed in 10 ml of the homogenates of the different organs and kept in a horizontal laboratory shaker. After 48 h, 500 μl of homogenate was removed, added to a chloroform–methanol mixture (chloroform:methanol = 4:1, 2 ml). After centrifugation at 4000 rpm for 20 min, the chloroform layers were collected and the concentrations of DOX were determined by high-performance liquid chromatography.

As shown in **Figure 9**, the DOX release in blood, heart, liver, spleen, lung and kidney is very slow, with less than 24% of DOX released after 48 h. The DOX release in Tumor is very fast, with more than 55%of DOX released after 48 h. This indicates that DOX in tumor can be released by the hydrolysis of GO@Au-PEG/DOX on hydrazone bond.

The weight change curve of mice in each group during treatment was shown in **Figure 10**. Only DOX group mice lost weight, while the weight of other mice did not. The weight loss of mice in DOX group was due to the low selectivity of chemotherapy drug DOX in treatment, which not only killed tumor cells but also caused damage to normal cells in the body, thus causing weight loss. The mice in the GO@Au-PEG/DOX+NIR group lost a little weight (still larger than the initial weight) at the end of treatment, which may be due to the effect of reduced tumor size on weight. At the later stage of treatment, the DOX group and the blank control group showed reduced activity and dull hair color, while the remaining 5 groups showed normal behavior and hair color. The results showed that the GO@Au-PEG prepared in the experiment had low toxicity and could be applied in vivo as a drug transport carrier, which could also improve the selectivity of chemotherapy drug DOX and reduce its toxic and side effects.

Tumor volume changes in each group during administration were shown in **Figure 11**. During the treatment, tumors in mice of normal saline group, saline + NIR group, GO@Au-PEG group were increased rapidly. At the end of the treatment, tumor volume in the saline group was about three times that at the beginning. No significant changes were observed in saline + NIR group and GO@Au-PEG group compared with the control group. This suggests that NIR irradiation alone could not effectively inhibit tumor growth and GO@Au-PEG alone was not effective in inhibiting tumor growth in the absence of NIR. The tumor volume in the GO@Au-PEG + NIR group at the end of administration was about 2.1 times that at the beginning of administration, indicating that GO@Au-PEG + NIR had a certain hyperthermia effect. Tumor growth was slow in the DOX group, and tumor volume at the end of administration was about 1.9 times that at the beginning of administration, indicating that chemotherapy alone could not effectively treat tumors. The tumor volume in the GO@Au-PEG/DOX group at the end of administration was about 1.1 times that at the beginning of administration, indicating that the GO@Au-PEG/DOX controlled release drug delivery system could deliver DOX to the tumor site with certain tumor targeting. The tumor volume of the GO@Au-PEG/DOX + NIR group at the end of administration was about 52% of that at the beginning of administration, and some of the tumors in mice had been completely eliminated, showing a significant tumor suppressive effect.

4 Conclusion

1. PEG can be successfully removed from the GO@Au-PEG system in a weak acidic environment, with good pH sensitivity. At the same time, under laser irradiation, the heating efficiency of GO@Au was significantly higher than that of GO alone, thus confirming that Go@Au-PEG has a good photothermal effect and can be used in the hyperthermia of tumors.
2. Under laser irradiation, GO@Au-PEG/DOX can release more DOX, and under certain conditions, DOX release is related to laser irradiation power, laser irradiation time, and the pH of the medium.

3. Go@Au-PEG system has little toxicity in vitro in the absence of laser irradiation, so it can be used as a drug carrier. However, in the absence of laser irradiation, the toxicity of GO@Au-PEG system on MCF-7 cells is significantly increased, showing a good photothermal treatment effect. The growth inhibition of MCF-7 in the GO@Au-PEG/DOX group was significantly increased after laser irradiation.
4. Go@Au-PEG was more likely to aggregate at tumor sites in mice, showing significant targeting. Under laser irradiation, GO@Au-PEG/DOX tumor targeted and controlled release drug delivery system had an obvious tumor suppressive effect. By the end of treatment, more than half of the tumors in mice had been completely eliminated, and tumor volume had decreased by about 52% on average, showing good effects of hyperthermia and chemotherapy.

5 Methods

The particle size, zeta potential and morphology of GO@Au-PEG/DOX were TEM were characterized by DLS and TEM. A UV-Vis spectrometer was used to characterize the optical properties of GO@Au-PEG and GO@Au-PEG/DOX. . Fourier transform infrared (FTIR) spectra were recorded with spectrophotometer. Au in GO@Au was measured with an inductively coupled plasma emission spectrometer (ICP). The photothermal efficacy of GO@Au-PEG/DOX was measured using a thermal infrared imager. An appropriate amount of sample powder was put into the platinum crucible, and the minimum temperature was set as 25℃, the maximum temperature as 800℃, and the temperature rising speed was set as 20℃/min. Under the protection of nitrogen, the samples were measured and recorded by thermal gravimetric analysis (TGA), and the PEG content in each sample was calculated.

To evaluate pH sensitivity, 10 mg samples were placed in phosphate buffer solutions with pH values of 7.4 and 5.5 respectively, centrifuged at room temperature for 4 h, and then dried at 60 ℃ for 24 h, and then the PEG content was measured by TGA.

The concentrations of DOX were measured at 480 nm by UV–Vis spectrometer. GO@Au-PEG/DOX was sealed in dialysis membranes (MW=8000~14000). The dialysis bags were incubated in 10 ml PBS buffer at 37 ℃ with a stirring rate of 100 r/min. A 200 μl portion of the aliquot was collected from the incubation medium at predetermined time intervals, and the released DOX was quantified by absorption spectroscopy recorded on UV Vis spectrophotometer at 490 nm. The dose released was quantified by collecting 200 μl portion of the aliquot from the culture medium at predetermined intervals and recording them with an UV-Vis spectrophotometer at 480nm. The DOX release studies were performed in triplicate for each of the samples.

5.1 Cellular Experiments

5.1.1 Cell Culture

Breast cancer MCF-7 cells were selected as experimental cells and cultured in a 37 ℃, 5% CO_2 incubator with RPMI1640 complete culture medium containing 10% fetal bovine serum and 1% streptomycin every 2~3 days for passage. The logarithmic growth cells were taken for the following experiments.

5.1.2 Cellular Uptake

MCF-7 cells were seeded at 3 × 10^5 cells/well on glass cover slips in 6-well plates. Cell plate was included in the cell culture box for 24 h. The cells were added into 2ml different pH containing media (DOX: 10 μg/ml, GO@Au-PEG: 12 μg/ml). The cells were cultured for 1, 2 and 4 h. The cells cultured for 4 h were irradiated with 808 nm laser (2 W/cm^2) for 10 min as a control experiment.

5.1.3 Cytotoxicity Assay

The cytotoxicity of DOX, GO@Au-PEG and GO@Au-PEG/DOX against MCF-7 cells was assessed by using the standard SRB assay. The MCF-7 cells were cultured and lifted as described above before seeding ($6×10^3$) into 96-well plates (5% CO_2, 37 ℃) and incubating for 24 h. When the cells were monolayer full of cell plate hole bottom, the original culture medium was taken out, and the medium containing different concentrations of drugs was added. 6 compound Wells were set at each concentration, and blank controls were set. The 96-well plates were taken out and the medium was moved out of the wells. Each well was washed three times with 100 L PBS buffer. Then 200 L precooled TCA solution with a final concentration of 10% was added to the wells. After fixing, wash with distilled water and dry naturally. Then, 0.4% SRB acetic acid solution of 100 L was added to each well for staining. The solution was allowed to stand at room temperature in darkness for 20min and then washed with 1% acetic acid.After drying, 10 mol/L Tris base solution of 150 L was added to each well. The cells were placed in an oscillator and oscillated at 37 ℃ for 10 min to dissolve the protein-bound SRB.Finally, the OD value of each well was measured at 515 nm with a microplate reader, so as to calculate the survival rate and inhibition rate of cells.

5.1.4 Statistical Analysis

Quantitative data are expressed as mean ± SD and analyzed by use of Student's *t* test. When *P* values < 0.05 were considered statistically significant.

Declarations

Ethics approval and consent to participate: Written informed consent was obtained from individual or guardian participants.

Consent for publication: Not applicable

Competing interests: The authors declare no interests conflicts.

Funding The Science and Technology Bureau of Fujian Province (No. 2019J01070); The Science and Technology Bureau of Quanzhou City (No. 2018Z012).

Authors' contributions: Mingqing Tang: Conceptualization, Methodology, Software, Investigation, Writing - Original Draft. Pengliang Xin: Validation, Formal analysis, Visualization, Software, Writing: Review &

Editing. Hongjun Lin: Validation, Formal analysis, Visualization.Writing: Review & Editing. Huangen Li: Resources, Writing - Review & Editing, Supervision,Writing: Review & Editing

Acknowledgement This work was funded by the Science and Technology Bureau of Fujian Province (No. 2019J01070); The Science and Technology Bureau of Quanzhou City (No. 2018Z012).

Availability of data and material: The data and materials is availability from the corresponding author

References

1. Rami-Porta R. Ball D, Crowley J, et al The IASLC Lung Cancer Staging Project: proposals for the revision of the T descriptors in the forthcoming (seventh) edition of the TNM classification for lung cancer. Journal of Thoracic Oncology, 2007, 2(7): 593–602.
2. Siegel RL. Miller K D, Jemal A. Cancer statistics. 2019. *CA: a cancer journal for clinicians, 2019, 69(1): 7–34.*.
3. Weinstein JN. Collisson E A, Mills GB, et al The cancer genome atlas pan-cancer analysis project. Nat Genet, 2013, 45(10): 1113.
4. The I. of Whole T P C A, *Genomes Consortium*. Pan-cancer analysis of whole genomes. Nature, 2020, 578(7793): 82.
5. Wagner AD. Syn N L X, Moehler M, *et al. Chemotherapy for advanced gastric cancer. Cochrane database of systematic reviews*, 2017 *(8)*..
6. Kong X. Dong B, Song X, et al Dual turn-on fluorescence signal-based controlled release system for real-time monitoring of drug release dynamics in living cells and tumor tissues. Theranostics, 2018, 8(3): 800.
7. Peters JT. Hutchinson S S, Lizana N, et al Synthesis and characterization of poly (N-isopropyl methacrylamide) core/shell nanogels for controlled release of chemotherapeutics. Chem Eng J, 2018, 340: 58–65.
8. Liu CC. Zhao J J, Zhang R, et al Multifunctionalization of graphene and graphene oxide for controlled release and targeted delivery of anticancer drugs. American journal of translational research, 2017, 9(12): 5197.
9. Kim J. Yung B C, Kim WJ, et al Combination of nitric oxide and drug delivery systems: tools for overcoming drug resistance in chemotherapy. J Controlled Release, 2017, 263: 223–30.
10. Vo AQ. Feng X, Morott JT, et al A novel floating controlled release drug delivery system prepared by hot-melt extrusion. Eur J Pharm Biopharm, 2016, 98: 108–21.
11. Du L. Yang S, Li W, et al Scaffold composed of porous vancomycin-loaded poly (lactide-co-glycolide) microspheres: A controlled-release drug delivery system with shape-memory effect. Materials Science Engineering: C, 2017, 78: 1172–8.
12. Huang X. Wu S, Du X. Gated mesoporous carbon nanoparticles as drug delivery system for stimuli-responsive controlled release. Carbon, 2016, 101: 135–42.

13. Luo Y. Liu Z, Zhang X, et al Effect of a controlled-release drug delivery system made of oleanolic acid formulated into multivesicular liposomes on hepatocellular carcinoma in vitro and in vivo. Int J Nanomed, 2016, 11: 3111.
14. Jiao X. Wang Z, Wang F, et al Dual Stimuli-Responsive Controlled Release Nanocarrier for Multidrug Resistance Cancer Therapy. ChemPhysChem, 2019, 20(24): 3271–5.
15. Feng Q. Zhang Y, Zhang W, et al Tumor-targeted and multi-stimuli responsive drug delivery system for near-infrared light induced chemo-phototherapy and photoacoustic tomography. Acta biomaterialia, 2016, 38: 129–42.
16. Bai S. Gao Y E, Ma X, et al Reduction stimuli-responsive unimolecular polymeric prodrug based on amphiphilic dextran-framework for antitumor drug delivery. Carbohydrate polymers, 2018, 182: 235–44.
17. Ding CD. Tong L, Fu JJ. Quadruple Stimuli-Responsive Mechanized Silica Nanoparticles: A Promising Multifunctional Nanomaterial for Diverse Applications. Chemistry–A European Journal, 2017, 23(60): 15041–5.
18. Zhou J. Tang Q, Zhong J, et al *Construction of glucose and H_2O_2 dual stimuli-responsive polymeric vesicles and their application in controlled drug delivery*. Journal of Materials Science, 2018, 53(20): 14063–74.
19. Alejo T. Andreu V, Mendoza G, et al Controlled release of bupivacaine using hybrid thermoresponsive nanoparticles activated via photothermal heating[J]. J Colloid Interface Sci, 2018, 523: 234–44.
20. Elbialy NS. Fathy M M, Reem ALW, et al Multifunctional magnetic-gold nanoparticles for efficient combined targeted drug delivery and interstitial photothermal therapy. International journal of pharmaceutics, 2019, 554: 256–63.
21. Jung HS. Verwilst P, Sharma A, et al Organic molecule-based photothermal agents: an expanding photothermal therapy universe. Chem Soc Rev, 2018, 47(7): 2280–97.
22. Nam J. Son S, Ochyl LJ, et al Chemo-photothermal therapy combination elicits anti-tumor immunity against advanced metastatic cancer. Nature communications, 2018, 9(1): 1–13.
23. Chen Q. Hu Q, Dukhovlinova E, et al Photothermal therapy promotes tumor infiltration and antitumor activity of CAR T cells. Adv Mater, 2019, 31(23): 1900192.
24. Oggu GS. Sasikumar S, Reddy N, et al Gene delivery approaches for mesenchymal stem cell therapy: strategies to increase efficiency and specificity. Stem Cell Reviews Reports, 2017, 13(6): 725–40.
25. Wang L. Hu Y, Hao Y, et al Tumor-targeting core-shell structured nanoparticles for drug procedural controlled release and cancer sonodynamic combined therapy. Journal of controlled release, 2018, 286: 74–84.
26. Xue Z. Zhu M, Dong Y, et al An integrated targeting drug delivery system based on the hybridization of graphdiyne and MOFs for visualized cancer therapy. Nanoscale, 2019, 11(24): 11709–18.
27. Wu M. Huang S. Magnetic nanoparticles in cancer diagnosis, drug delivery and treatment. Molecular clinical oncology, 2017, 7(5): 738–46.

28. Shi S. Zhang L, Zhu M, et al Reactive oxygen species-responsive nanoparticles based on peglated prodrug for targeted treatment of oral tongue squamous cell carcinoma by combining photodynamic therapy and chemotherapy. ACS Appl Mater Interfaces, 2018, 10(35): 29260–72.

Figures

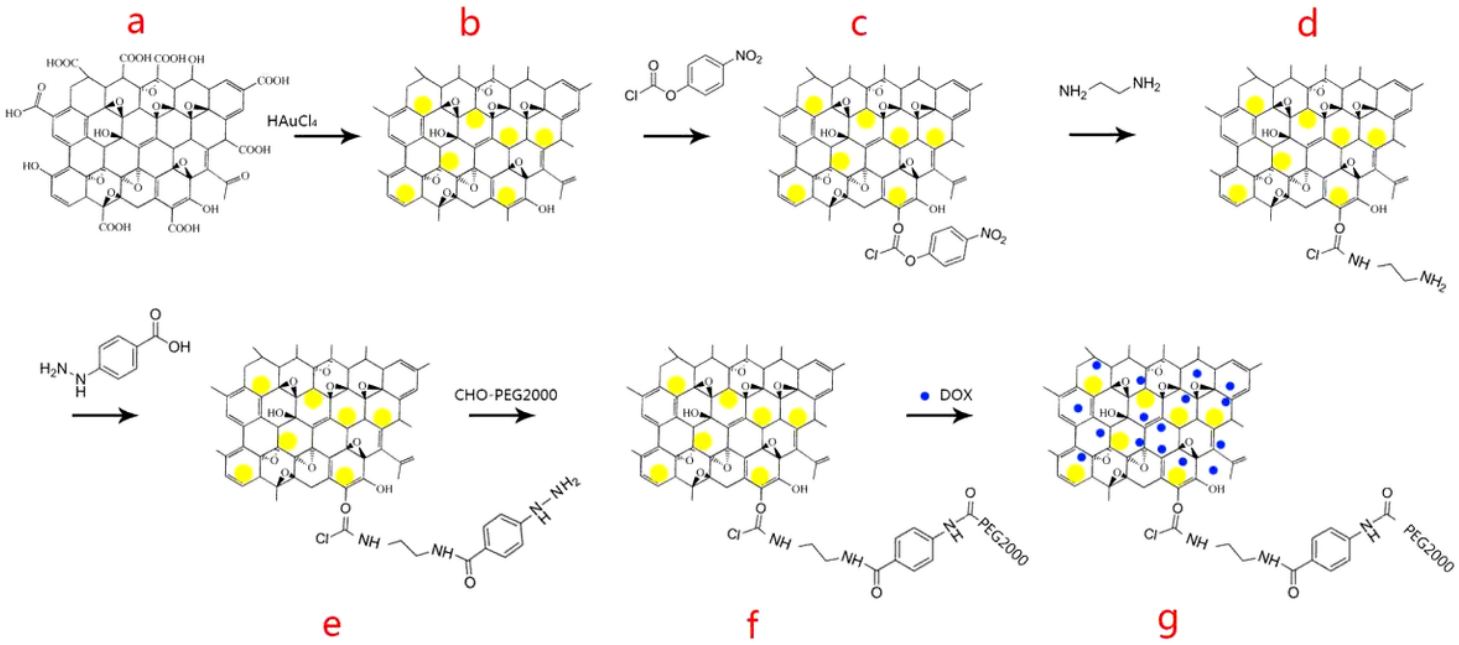

Figure 1

Schematic illustration of the synthetic steps from GO to GO@Au-PEG/DOX.

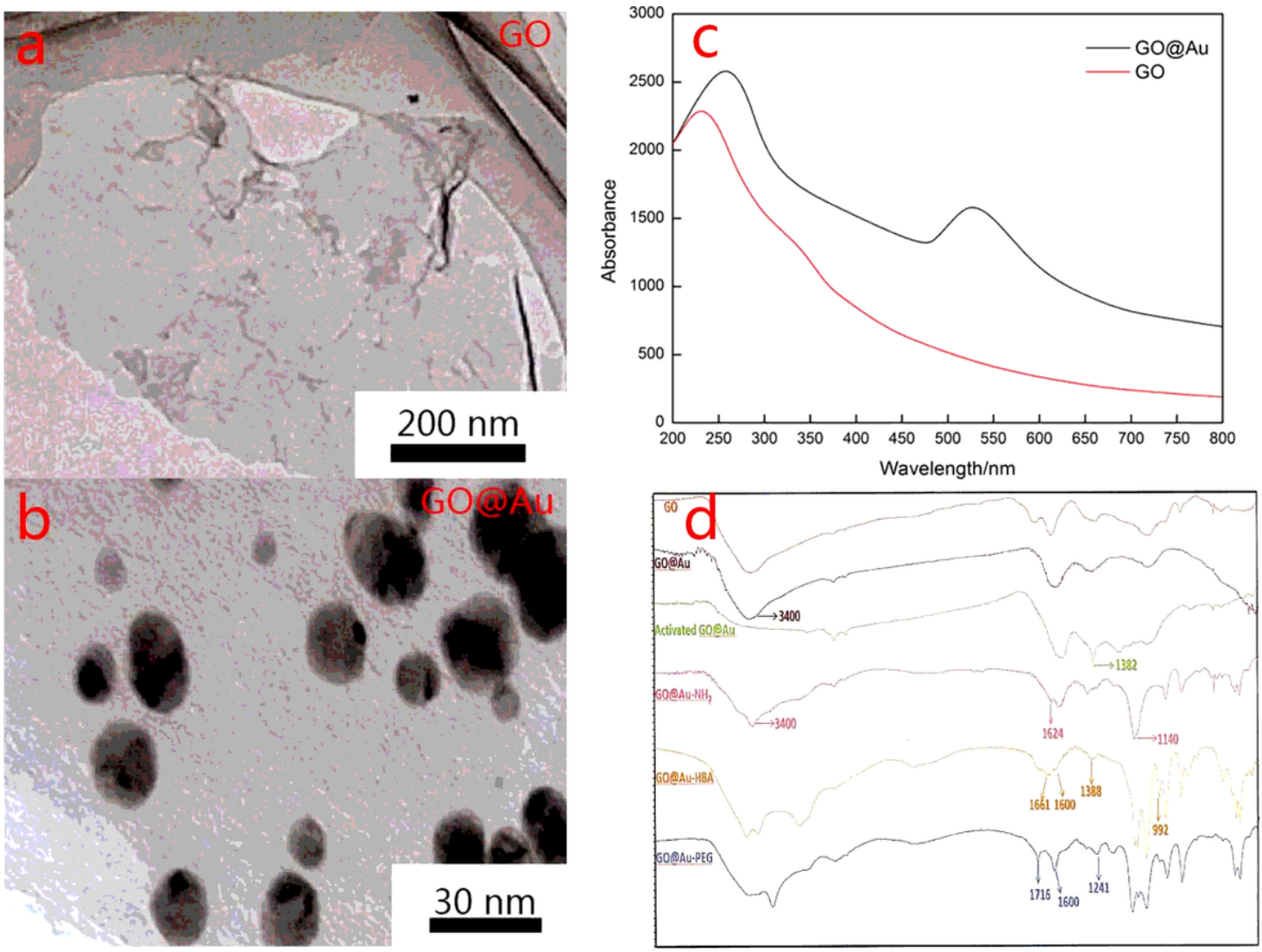

Figure 2

Characterization of GO@Au-PEG. (a) TEM image of GO, (b) TEM image of GO@Au, (c) UV–Vis spectrum of GO and GO@Au, (d) FT-IR spectrum of GO, GO@Au, activated GO@Au, GO@Au-NH2, GO@Au-HBA and GO@Au-PEG.

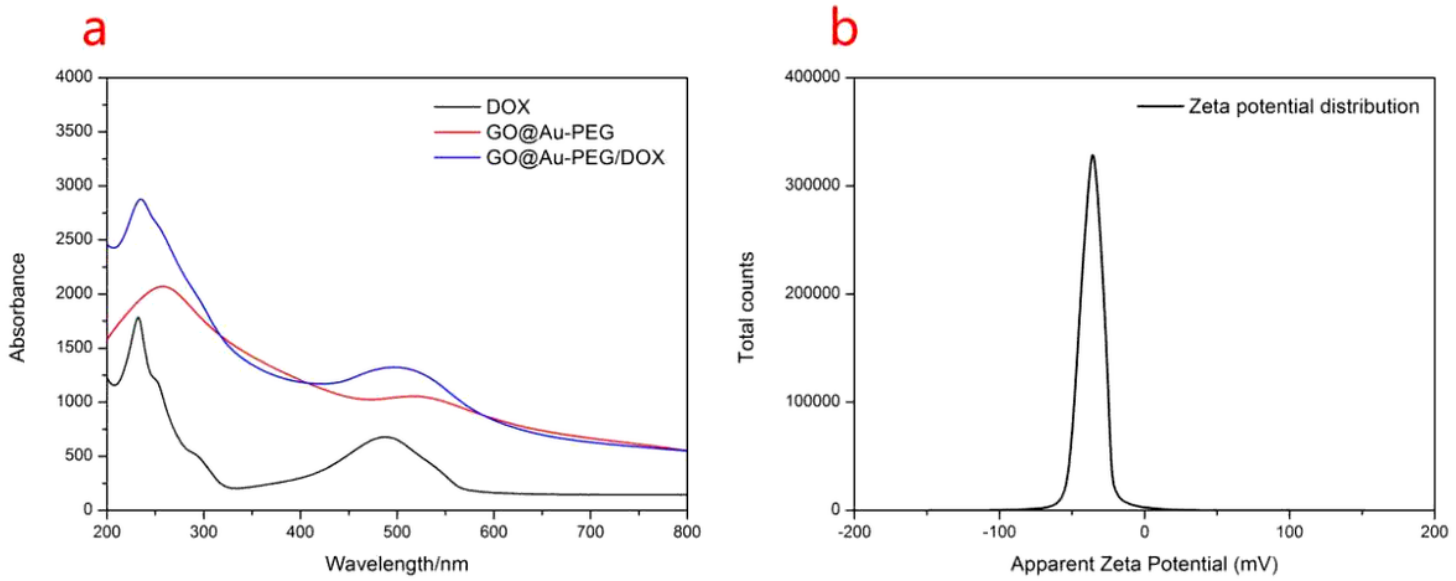

Figure 3

Characterization of GO@Au-PEG/DOX. (a) UV–Vis spectrum of DOX, GO@Au-PEG and GO@Au-PEG/DOX, (b) Zeta potential distribution of GO@Au-PEG/DOX.

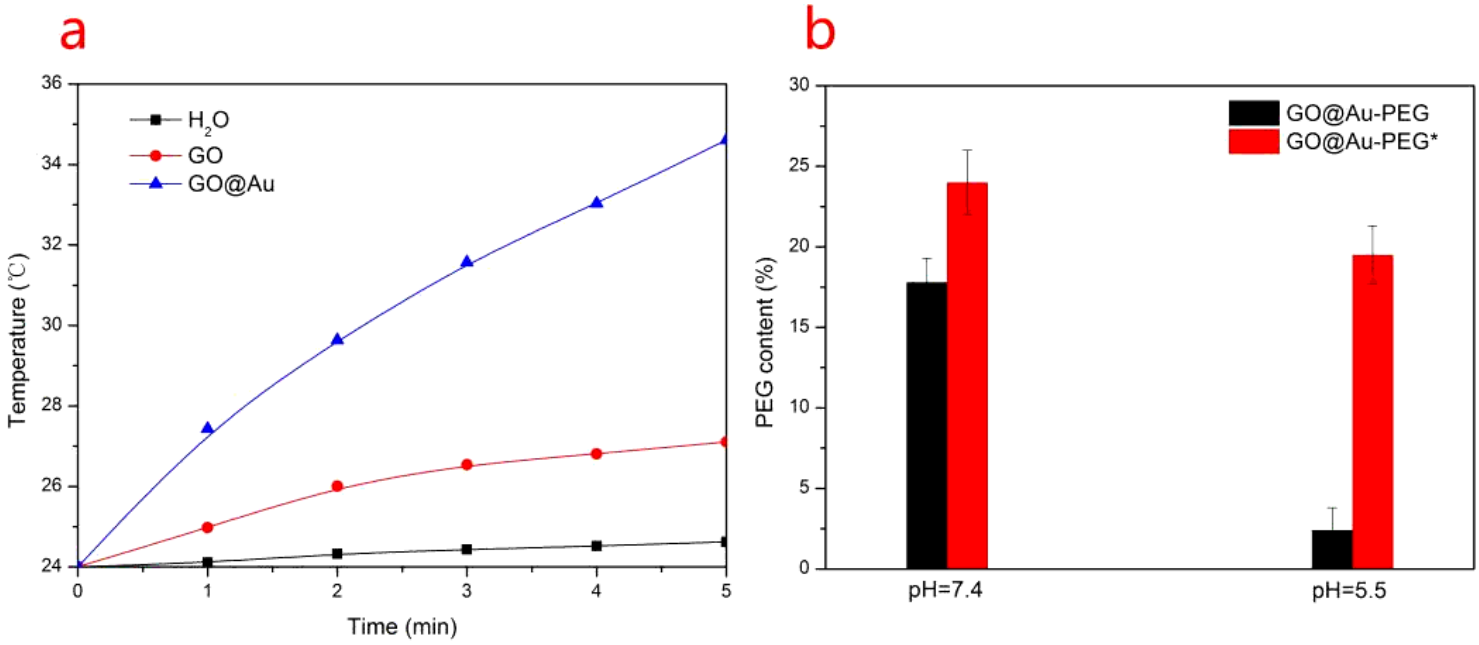

Figure 4

Photothermal effect and pH sensitivity. (a) The temperature changes of GO and Go@Au under laser irradiation(808 nm, 2 W/cm2, 5 min), (b) PEG content changes in GO@Au-PEG and GO@Au-PEG* at different pH values for 4h.

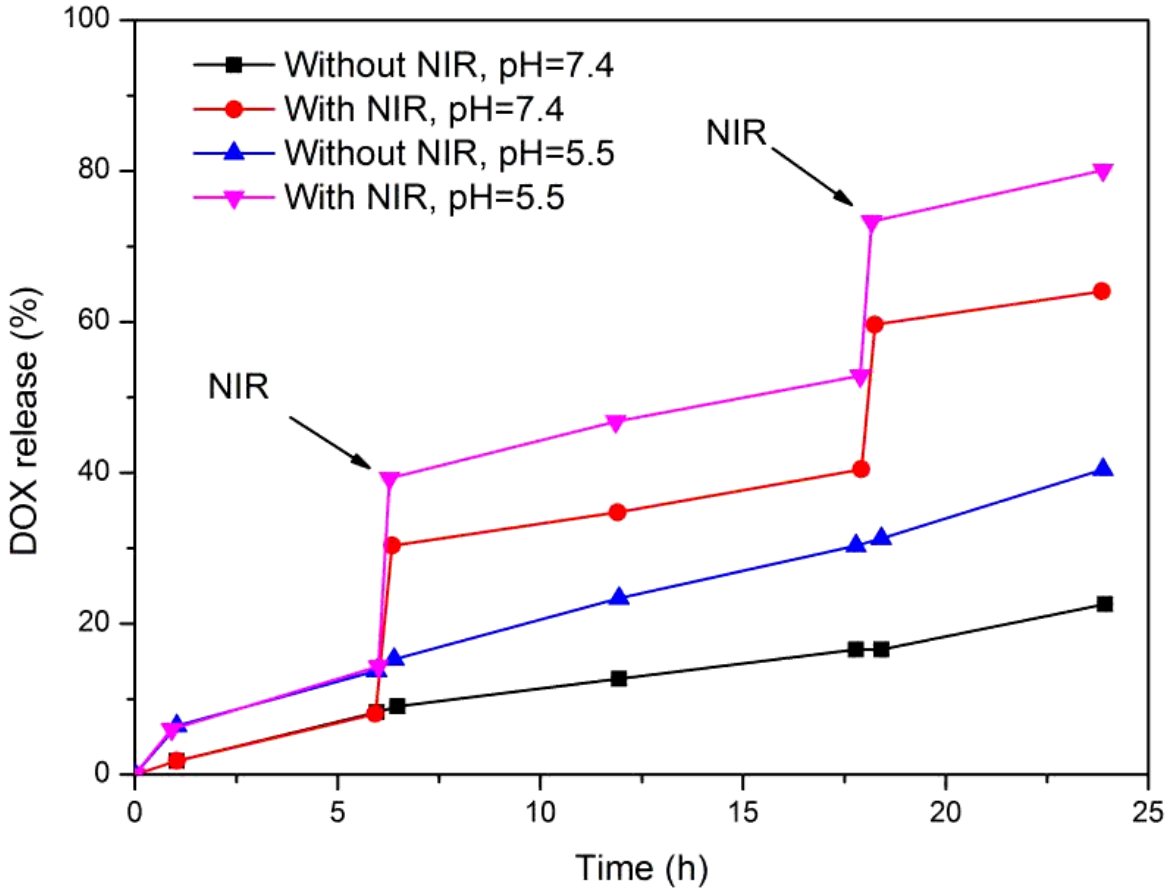

Figure 5

DOX release results within 24 h under different pH. NIR radiation (808 nm, 2 W/cm2, 20 min) was performed at 6 h and 18 h.

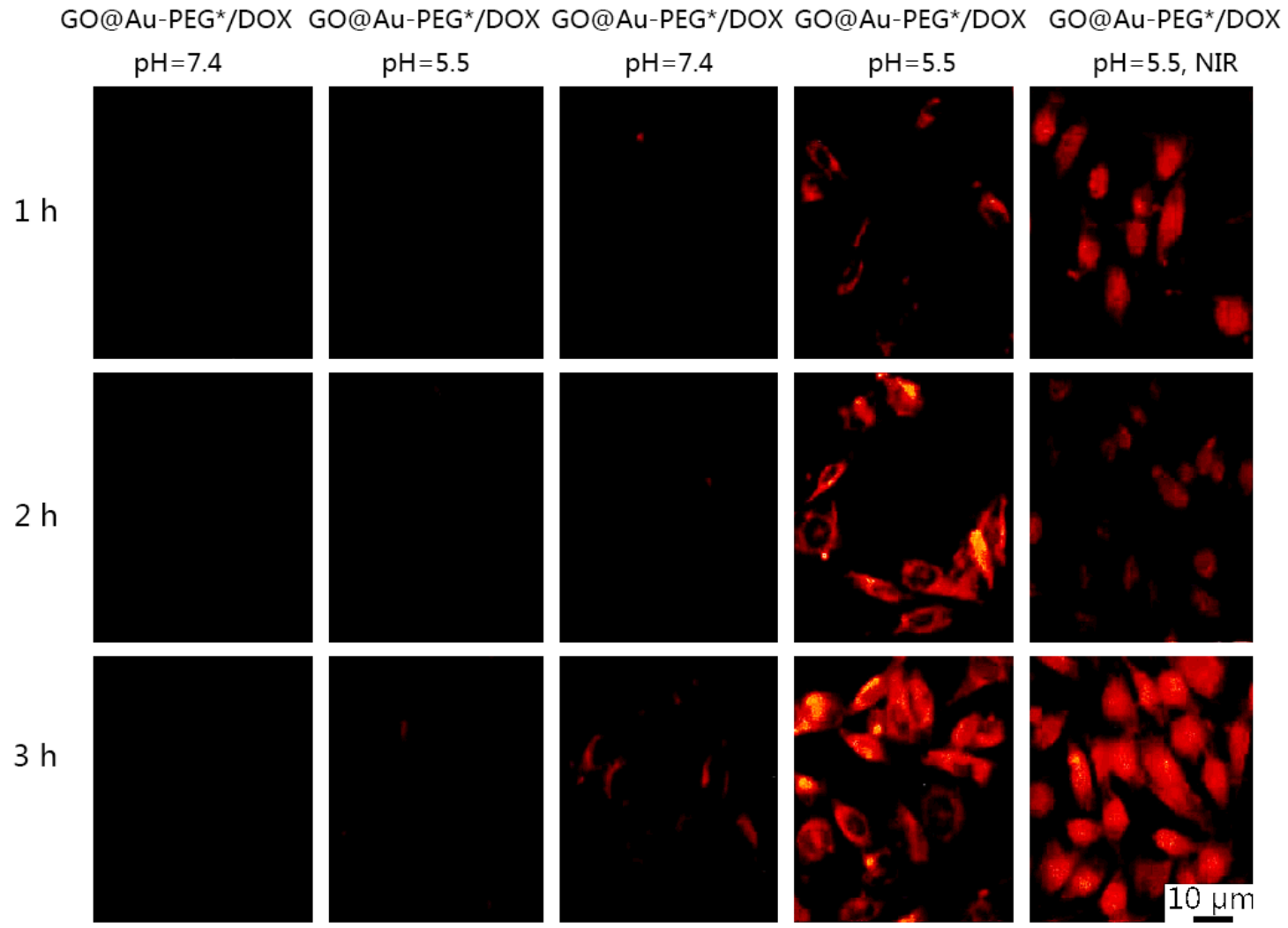

Figure 6

Fluorescence images of MCF-7 cells incubated with GO@Au-PEG*/DOX and Go@Au-PEG/DOX for 1, 2 and 4 h with and without NIR (808 nm, 2 W/cm2).

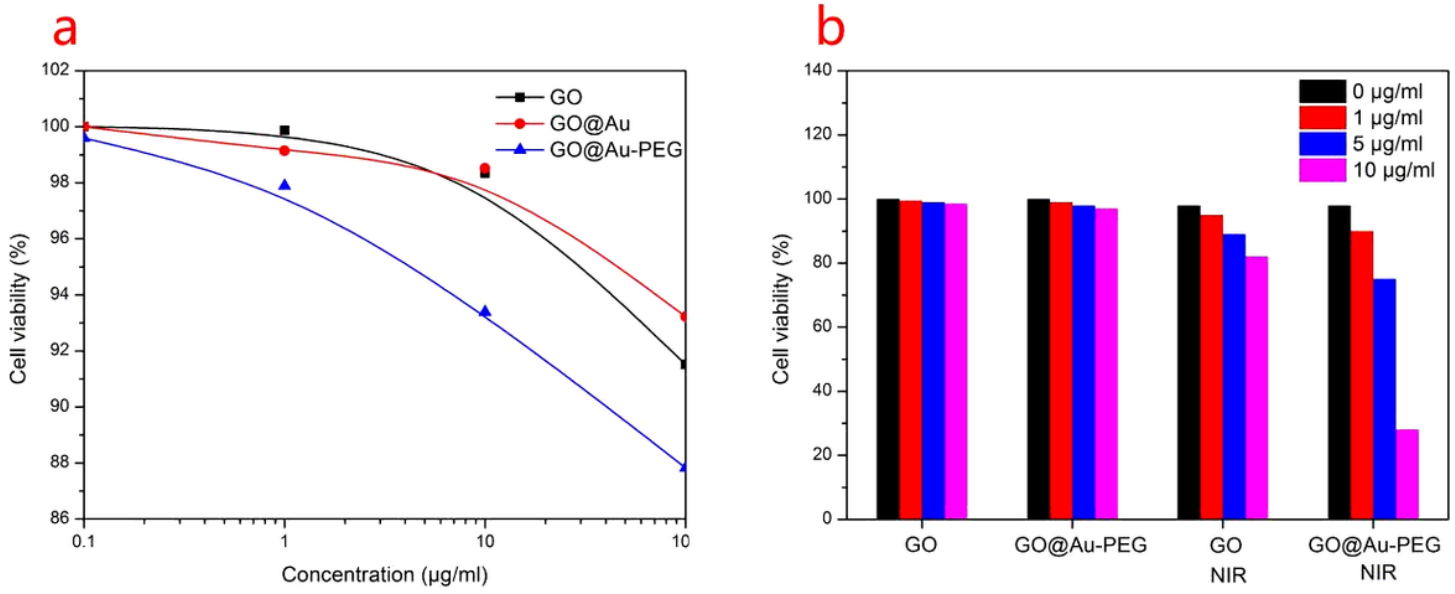

Figure 7

Cell viability under different conditions. (a) Cytotoxicity of GO, GO@Au and GO@Au-PEG on MCF-7 cells at 24 h, (b) Cytotoxicity of GO and GO@Au-PEG at different concentrations to MCF-7 cells with or without NIR irradiation (808 nm, 2 W/cm2).

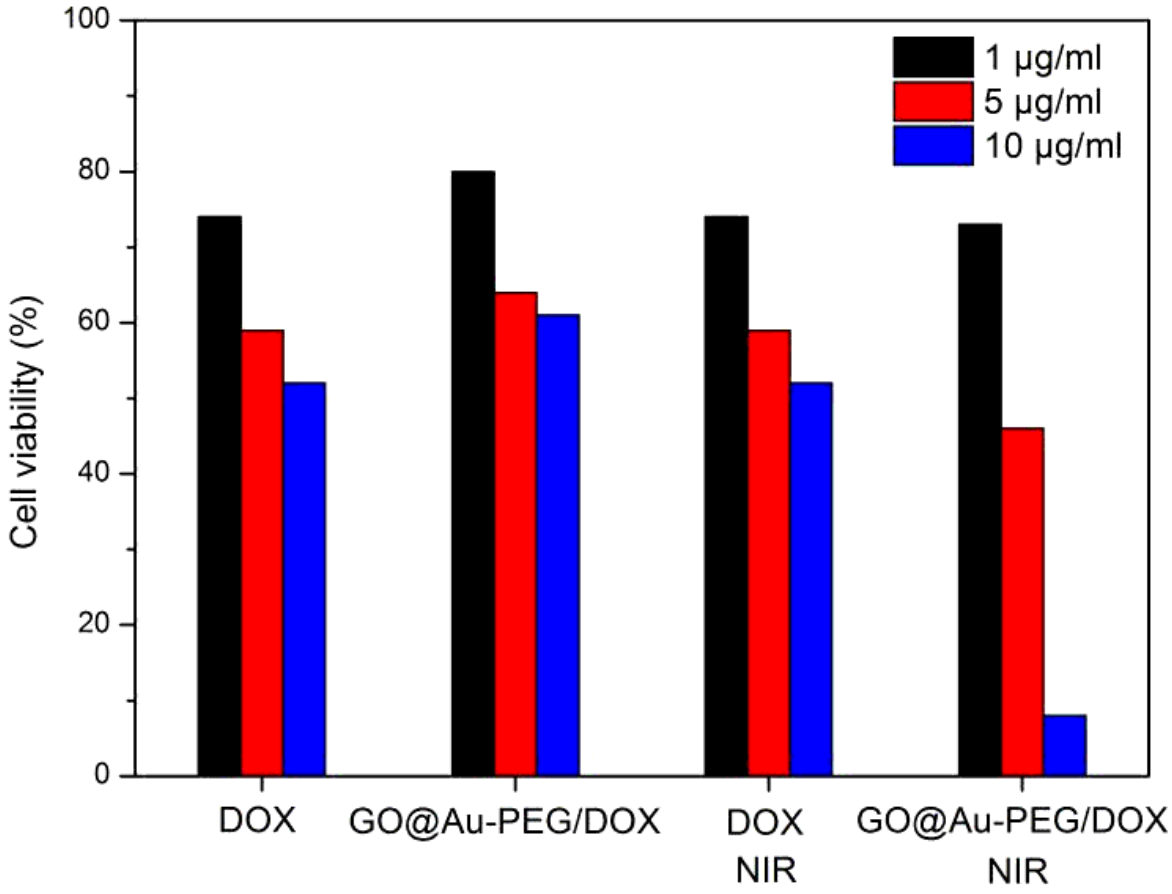

Figure 8

Cytotoxicity of DOX and GO@Au-PEG/DOX on MCF-7 cells at 24 h with and without NIR irradiation (808 nm, 2 W/cm2).

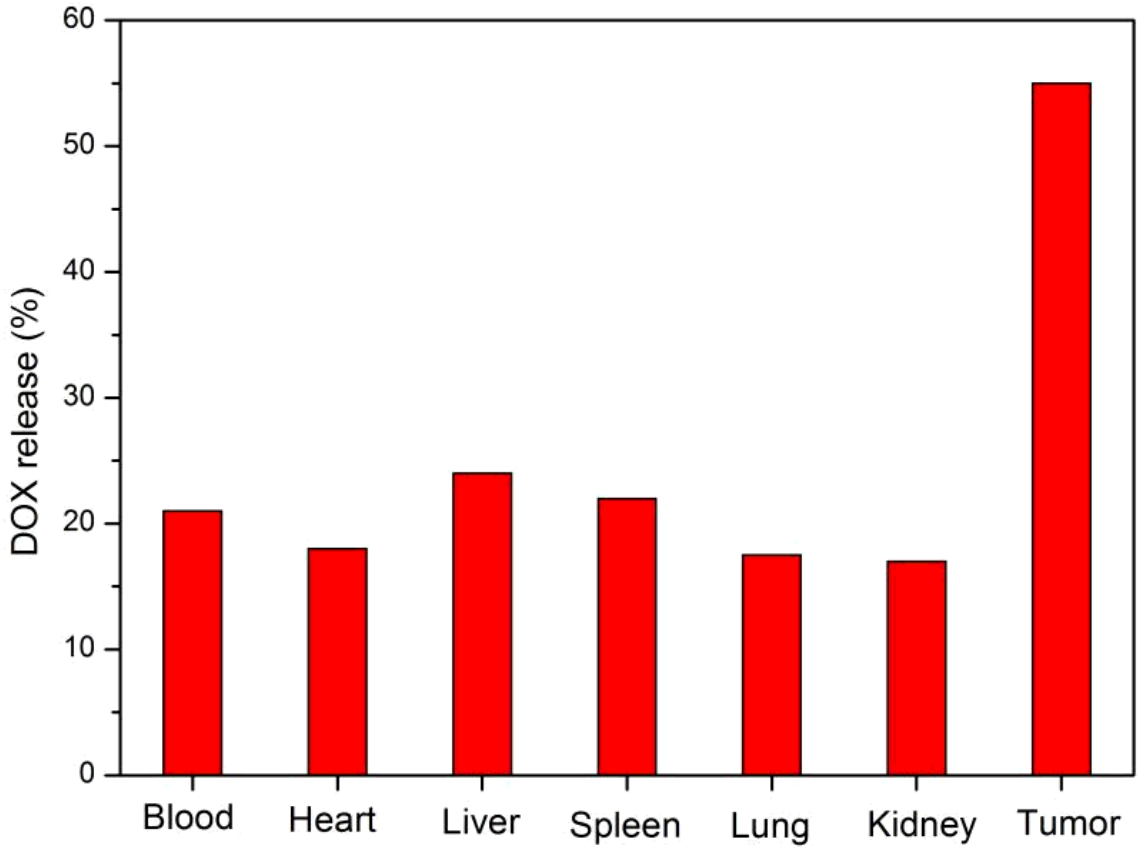

Figure 9

DOX release from GO@Au-PEG/DOX in different tissues for 2 d.

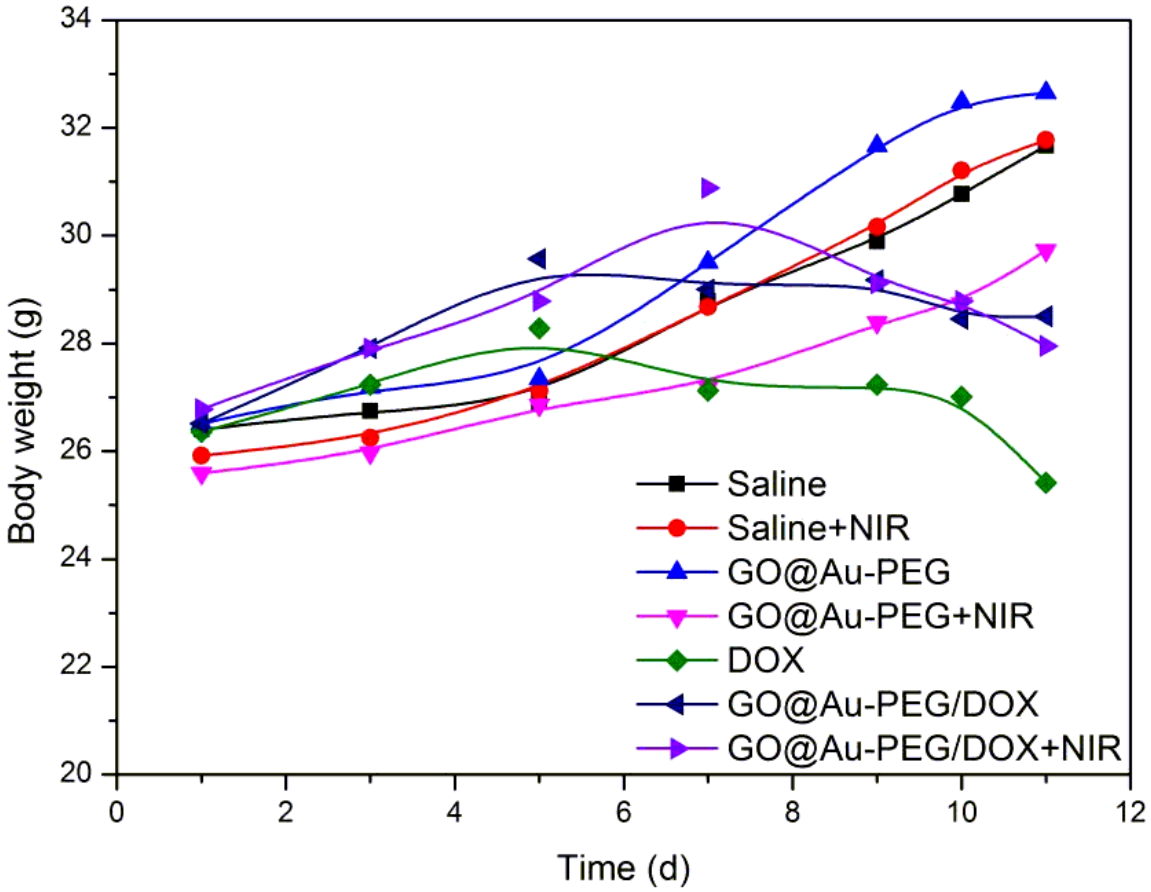

Figure 10

Changes in body weight over time in mice.

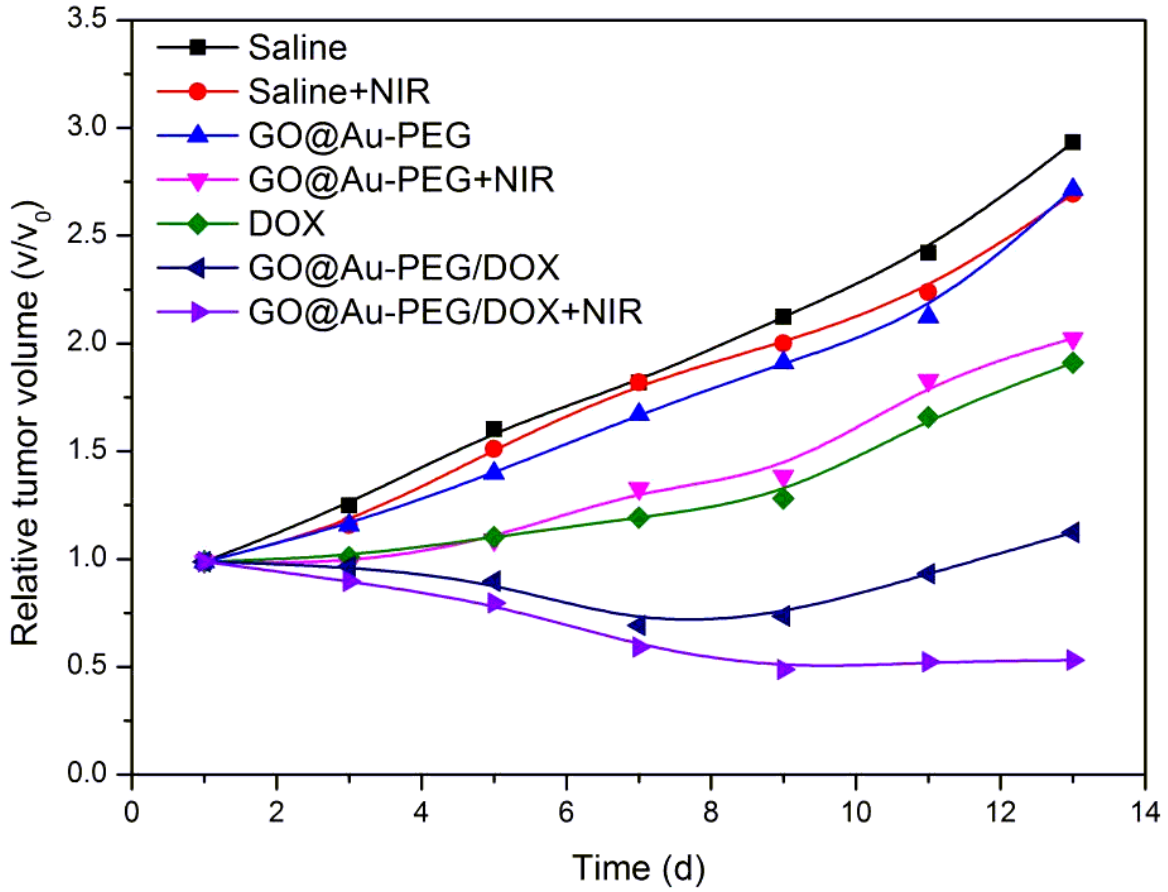

Figure 11

Changes in tumor relative volume.